Title

Variability in diatom contributions to biomass, organic matter production and export across a frontal gradient in the California Current Ecosystem

Journal

Journal of Geophysical Research - Oceans, 120(2)

ISSN

2169-9275

Authors

Krause, Jeffrey W
Brzezinski, Mark A
Goericke, Ralf
et al.

Publication Date

2015-02-01

DOI

10.1002/2014jc010472

Peer reviewed

AGU PUBLICATIONS

JGR

Journal of Geophysical Research: Oceans

RESEARCH ARTICLE

10.1002/2014JC010472

Key Points:
- Eddy interactions led to variability comparable to basin-scale variability
- Diatoms' contribution to production rates were higher than to autotrophic biomass
- Diatom growth in a cyclonic eddy was likely limited by iron availability

Supporting Information:
- Supporting Information S1
- Data Set S1
- Data Set S2
- Data Set S3
- Data Set S4

Correspondence to:
J. W. Krause,
jkrause@disl.org

Citation:
Krause, J. W., M. A. Brzezinski, R. Goericke, M. R. Landry, M. D. Ohman, M. R. Stukel, and A. G. Taylor (2015), Variability in diatom contributions to biomass, organic matter production and export across a frontal gradient in the California Current Ecosystem, *J. Geophys. Res. Oceans*, *120*, 1032–1047, doi:10.1002/2014JC010472.

Received 24 SEP 2014
Accepted 22 JAN 2015
Accepted article online 27 JAN 2015
Published online 20 FEB 2015

Variability in diatom contributions to biomass, organic matter production and export across a frontal gradient in the California Current Ecosystem

Jeffrey W. Krause[1,2], Mark A. Brzezinski[1,3], Ralf Goericke[4], Michael R. Landry[4], Mark D. Ohman[4], Michael R. Stukel[5,6], and Andrew G. Taylor[4]

[1]Marine Science Institute, University of California, Santa Barbara, California, USA, [2]Dauphin Island Sea Lab, Dauphin Island, Alabama, USA, [3]Department of Ecology Evolution and Marine Biology, University of California, Santa Barbara, California, USA, [4]Scripps Institution of Oceanography, University of California at San Diego, La Jolla, California, USA, [5]Horn Point Laboratory, University of Maryland, Cambridge, Maryland, USA, [6]Now at Earth, Ocean, and Atmospheric Science Department, Florida State University, Tallahassee, Florida, USA

Abstract In the offshore waters of Southern California, submesoscale processes associated with fronts may stimulate phytoplankton blooms and lead to biomass shifts at multiple trophic levels. Here we report the results of a study on the cycling of biogenic silica ($bSiO_2$) with estimates of the contributions of diatoms to primary and new production in water masses adjacent to (i.e., coastal or oceanic) and within an offshore front in the Southern California Current Ecosystem (CCE). The coastal and oceanic water were sampled in cyclonic and anticyclonic eddies, respectively, with the frontal water being an interaction region between the eddy types. Concentrations of $bSiO_2$ varied by 25-fold across the front, with concentrations in frontal waters 20–25% of those in coastal waters. Rates of biogenic silica production spanned an equally large range, with rates within the frontal region that were half those in the coastal regions. Contributions of diatoms to primary and new production were disproportionately higher than their contribution to autotrophic biomass in all areas, ranging from 5–8%, 19–30%, and 32–43% for both processes in the oceanic, frontal and coastal waters, respectively. Across the frontal area, diatoms could account for $<$1.0%, 6–8%, and 44–72% of organic matter export in the oceanic, frontal and coastal waters, respectively. The results suggest that the regions of frontal interactions between eddies in the southern CCE can account for variability in diatom biomass, productivity and export over very short spatial scales that is comparable to the variability observed across the Pacific basin.

1. Introduction

The California Current Ecosystem (CCE) is a biologically productive upwelling region along the western coast of the North American continent. The predominant southward flow of the California Current brings cool waters down the coast from the North Pacific. During spring and summer months, winds are favorable for offshore Ekman flow, resulting in near-shore upwelling of high-nutrient waters and intense diatom blooms along the central California coast north of Pt. Conception [*Lassiter et al*., 2006]. Along the southern California coast (south of Pt. Conception), strong near-shore upwelling is typically not observed, and the complex hydrography also gives rise to mesoscale features (e.g., eddies and fronts), which are readily identifiable using remote observations of sea-surface temperature and chlorophyll a up to 500–700 km offshore [*Kahru et al*., 2012].

Generally speaking, mesoscale features can be disproportionately important for processes like primary productivity, nutrient cycling and trophic ecology relative to their areal extent [e.g., *Nelson et al*., 1985; *Yoder et al*., 1994; *Powell and Ohman*, 2015]. Within these features, diatom growth can be stimulated, resulting in biomass accumulations, in some cases, well above those of adjacent waters [e.g., *Taylor et al*., 2012]. Such responses are not limited to coastal regions, as open-ocean mesoscale eddies may contain diatom communities with 1–2 orders-of-magnitude higher biomass than waters outside the eddy [*Benitez-Nelson et al*., 2007; *McGillicuddy et al*., 2007; *Krause et al*., 2009a, 2010b]. Fronts in the North Pacific have been shown to accumulate larger diatom cells and chains, which potentially stimulate production and biomass of higher trophic level organisms in the pelagic or benthic environments [*Yoder et al*., 1994; *Smith et al*., 1996]. While

CCE waters generally have higher diatom standing stocks compared to the open ocean, proportionately similar levels of diatom-biomass enhancement have been observed at fronts in this region [*Taylor et al*., 2012].

Recent observations in the offshore waters of Southern California have demonstrated the potential importance of deep-water fronts in the CCE. In the "A-Front" study, for example, *Li et al*. [2012] suggested that autotrophic biomass accumulation at the front was driven by increased nitrate flux into the euphotic zone, which enhanced primary production, coupled with reduced grazing by microzooplankton. Among photoautotrophs, diatoms especially increased at the front to two to three fold higher biomass than the adjacent assemblage on the coastal side of the front and over an order of magnitude higher than the oceanic side of the front [*Taylor et al*., 2012]. The diatom-dominated frontal region was also associated with a transformed food web. Abundances of calanoid copepods, nauplii, euphausiids and appendicularians were notably higher at the front than in adjacent coastal and oceanic waters [*Ohman et al*., 2012]. Acoustic analysis also demonstrated enhancement of vertically migrating groups of euphausiids, larval fish and mesopelagic fish [*Lara-Lopez et al*., 2012]. In addition, in situ imaging showed several-fold higher concentrations of large organic aggregates in the A-Front area relative to outside waters [*Ohman et al*., 2012]. Since large aggregates may sink rapidly [e.g., *Alldredge and Gotschalk*, 1988], their elevated presence implies that enhanced organic matter export can be important at fronts.

Despite these compelling observations, there is little understanding of rate variability and elemental cycling across frontal gradients in this region. Fronts are areas of water mass interaction, hence, the biological response in such regions depends on a combination of the initial communities present, the physical and chemical properties of the interacting water masses, and the external physical forcing (e.g., wind direction and magnitude). A phytoplankton species shift, e.g., from dominance by nano and picoplankton to microplankton, may or may not significantly increase community primary productivity (e.g., factor 2 and 3), but the impact on regional new production or export flux could be much higher, as larger cells (e.g., diatoms, dinoflagellates) typically contribute more significantly to these processes. Thus, the biogeochemical implications of diatom biomass and growth variability across frontal gradients in the CCE may be substantial.

Here we report results from a cruise that combined quasi-Lagrangian process studies and high-resolution transect sampling through a frontal region between an anticyclonic and cyclonic eddy. Given previous findings (e.g., A-Front), we focus on spatial variability in diatom growth and their contributions to total organic-matter production and export rates across the frontal gradient. To assess diatoms specifically, we utilize their obligate requirement for silicon, which they use to make a frustule of amorphous biogenic silica ($bSiO_2$), and track changes in the rates of $bSiO_2$ production and export and the role of silicic acid ($Si(OH)_4$) concentrations in limiting uptake by diatoms. This information allows us to estimate the relative contributions of diatoms to the total rates of primary and new production, and to quantify how the biogeochemical role of diatoms changes across a frontal gradient in the southern CCE.

2. Methods

The P1106 cruise was conducted aboard the R/V *Melville* from 18 June through 17 July, 2011 ~150 km to the southwest of Point Conception, California (Figure 1). The cruise track was located in the northern domain of the California Cooperative Oceanic Fisheries Investigations study region [*Koslow et al*., 2011]. Lagrangian-style process studies and a high-resolution spatial transect were conducted at locations determined by real-time 3-D monitoring of environmental conditions using SeaSoar and a Moving Vessel Profiler [*Ohman et al*., 2013]. Similar Lagrangian-style experimental designs have been conducted on previous CCE Long-Term Ecological Research (LTER) process cruises, and have been discussed elsewhere in detail [*Landry et al*., 2009, 2012; *Ohman et al*., 2012].

A total of six Lagrangian-style process studies (termed experimental "cycles") were conducted within three regions—the open-ocean and coastal waters adjacent to the front and within the front itself. Later analysis of satellite-derived sea-level anomaly (SLA) data determined that the oceanic stations were associated with an anticyclonic eddy (positive SLA; Figures 1a and 1d), the coastal stations near or within two distinct cyclonic eddies (negative SLA; Figures 1b and 1c), and the frontal stations were located within the interacting regions between the anticyclone and both cyclones (Figures 1a and 1d). For brevity, the oceanic/anticyclone, frontal interaction, and coastal/cyclone cycles will be referred to as oceanic, frontal and coastal,

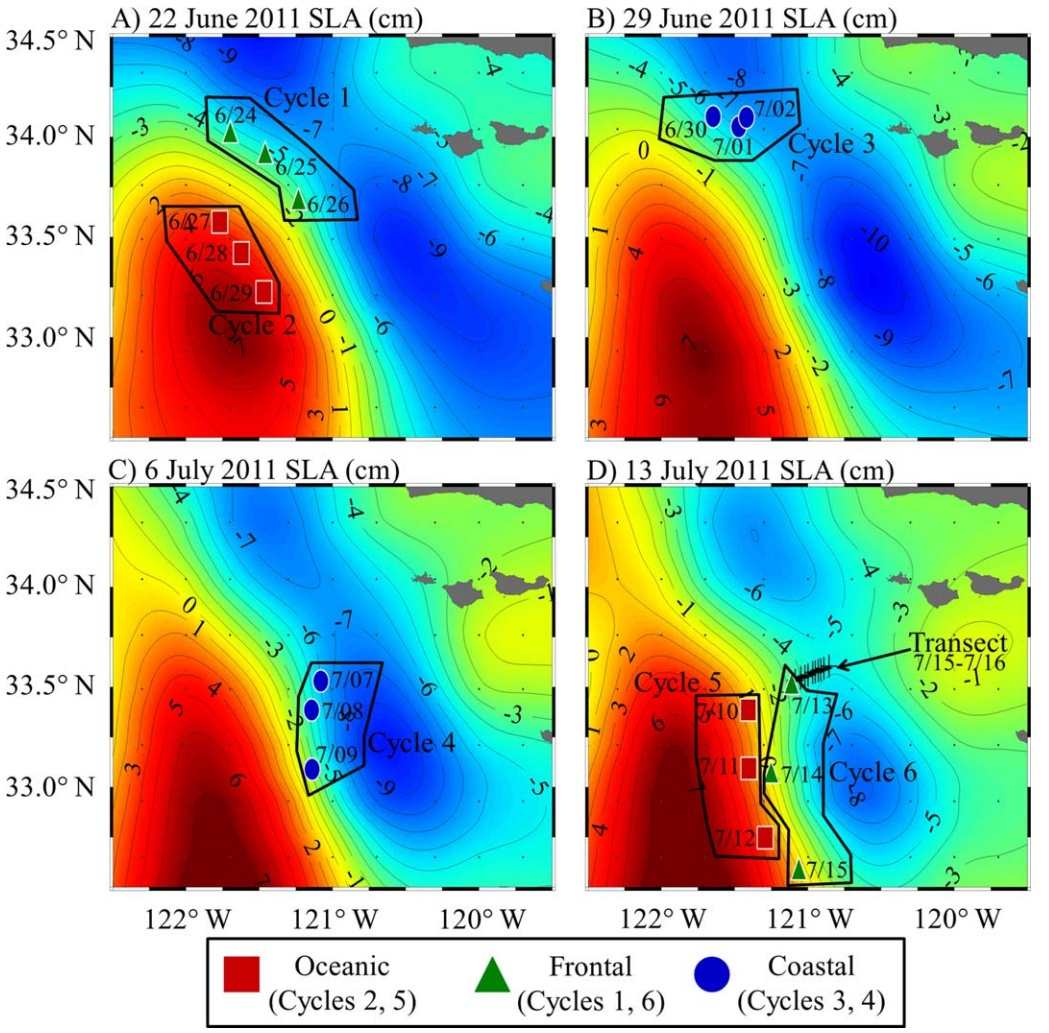

Figure 1. Map of sea level anomaly (cm) in the study area for P1106 cruise. Maps are for: (a) 22 June, (b) 29 June, (c) 6 July, and (d)13 July 2011, dates for each process station are listed (M/DD). Symbols represent the different cycle types: oceanic (squares), frontal (triangles) and coastal (circles) or the C-Front transect (crosses, Figure 1d). The altimeter products were produced by Ssalto/Duacs and distributed by Aviso (http://www.aviso.oceanobs.com).

respectively. Each cycle lasted 3 days, starting near midnight of Day 1 with the deployment of a drift array with VERTEX-style acrylic sediment traps (with a holey-sock drogue centered at 15 m [*Stukel et al*., 2013]). Hydrocasts for stock and rate measurements were conducted on Days 1 and 2 of each cycle, with Day 3 activity limited to stock measurements prior to the retrieval of drifting equipment. The hydrocasts discussed here were conducted predawn (typically ~02:00 local time) with CTD data profiles to depths of 500 m and Niskin-bottle sampling of water in the upper 40–100 m, depending on water-column properties. After experimental bottles were filled from the Niskin rosette, tracer was added and the bottles were placed into mesh bags and secured to an in situ surface-tethered productivity array at the depth where the water sample was taken. The sampling, processing and array deployment were all done prior to sunrise. After 24 h, Day 1 incubated samples from the array were retrieved and Day 2 experiments, collected and prepared in the same manner, were secured to the array and redeployed. The final (Day 3) retrieval of the incubation array was followed by retrieval of the sediment traps prior to departure for the next experimental cycle location. Tracer samples were processed immediately upon retrieval, and sediment trap samples were processed within a few hours.

In addition to the process studies, three high-resolution transects were conducted across the front from local sunset to sunrise at ~3 km spatial resolution. For logistic reasons, only standing stock measurements were made in the upper 85 m. Transect A sampling was halted prior to completion and transect B was

unsuccessful in capturing all three regions associated with the front. Here we report the results of transect C conducted between 15 and 16 July 2011 (hereafter referred to as "C-Front").

Macronutrients and biogenic particles were measured at every sampling depth during the experimental cycles and C-Front transect. For nutrients, water was sampled directly from the Niskin bottles after filtration though a 0.1 μm capsule filter (Suporcap). One aliquot of the filtrate was immediately frozen for autoanalyzer analysis (NO_3, NO_2, NH_4, PO_4) on shore, while the other was refrigerated at 4°C until analysis of $Si(OH)_4$ (<4 h) at sea using a sensitive manual colorimetric method [*Brzezinski and Nelson*, 1995]. Seawater for $bSiO_2$ analysis was collected (0.6 or 1.2 L depending on location), filtered through a 0.6 μm polycarbonate filter, placed in cryovials and dried in an oven for ~24 h. On land, samples were analyzed using a NaOH digestion procedure [*Brzezinski and Nelson*, 1995] in Teflon tubes, which provide low and stable blanks [*Krause et al*., 2009b]. Chlorophyll a (Chl a) concentration was determined by filtering 250 mL through glass fiber filters, extracting in 90% acetone in the dark at −18°C for 24 h and reading on a Turner 10AU fluorometer [*Strickland and Parsons*, 1972]. At the transect stations, samples were taken for assessment of nano and microplankton abundance according to the detailed protocol described in *Taylor et al*. [2012], which allows quantification of total carbon associated with autotrophic groups (e.g., diatoms, dinoflagellates, prymnesiophytes, etc.), and we specifically focus on diatom carbon.

The rate of biogenic silica production (ρ_P) was measured using the radioisotope ^{32}Si. Prior to the cruise, the entire isotope stock was cleaned of trace metals by passage through Chelex resin (BioRad). Cruise samples were collected directly from the Niskin bottles into polycarbonate bottles (150 mL or 300 mL), and 360 Bq of high specific activity $^{32}Si(OH)_4$ (>40 kBq μmol Si^{-1}) were added. The experimental bottles were kept in the dark during preparation and placed into mesh bags for deployment on the productivity array. After the 24 h in situ incubation at the depth of sample collection, the bottle contents were filtered (0.6 μm pore, 25 mm diameter polycarbonate filter) and the filters were mounted on a nylon disc and covered with Mylar after drying. The filters were processed using gas-flow proportional counting when ^{32}Si and its daughter isotope ^{32}P were at secular equilibrium [*Krause et al*., 2011a]. The specific rate of silica production (V_b) for each sample was calculated by normalizing ρ_P to [$bSiO_2$] at the corresponding depth using the equations described in *Brzezinski and Phillips* [1997]. The average V_b for the upper water column (V_{AVE}) was calculated by vertically integrating V_b to a specific depth (e.g., 40 m) then dividing by the depth of integration.

Gross rates of primary and new production are used to constrain the contributions of diatoms to each rate. Conversion of diatom ρ_P to diatom-specific primary production and new production were done using established approaches [*Krause et al*., 2011b]. Total community primary production and new production were measured using ^{14}C and $^{15}NO_3$-tracer methods, according to standard protocols for the CCE LTER program (http://cce.lternet.edu/data/methods-manual).

In each region, one experiment was conducted to assess the potential limitation of Si uptake by ambient silicic acid availability. Si uptake by diatoms in the laboratory and field populations conforms to Michaelis-Menten kinetics, described by the hyperbolic function:

$$V_b = \left(V_{MAX} \times \left[Si(OH)_4\right]\right) / \left(K_S + \left[Si(OH)_4\right]\right) \quad (1)$$

where V_{MAX} is the maximum theoretical uptake at nonlimiting [$Si(OH)_4$] and K_S is the [$Si(OH)_4$] where $V_b = {}^1/_2 V_{MAX}$, i.e., the half-saturation parameter. These experiments were performed at each station using water from <20 m depth to examine the response of Si uptake to eight silicic acid concentrations (i.e., ambient to +20 μmol L^{-1}). Seawater for each experiment was sampled directly from the CTD rosette into a single polycarbonate container and gently mixed just prior to being subsampled into 300 mL polycarbonate bottles. Radioisotope additions were the same as used on the production array, but kinetic experiment samples were incubated for 10 h on deck in a screened incubator (~50% of surface light) cooled by flowing surface seawater. After 10 h incubations, samples were processed as described above. Nonlinear regression analysis was performed in Sigmaplot 12.0 © software to fit the 8-point data set to the Michaelis-Menten function in order to calculate V_{MAX} and K_S and the associated standard error for each parameter.

Biogenic silica export was measured using a free-drifting sediment trap array [e.g., *Brzezinski et al*., 2011; *Stukel et al*., 2013]. Prior to deployment, collector tubes fitted with entrance baffles were filled with brine (50 g L^{-1} NaCl in 0.2 μm filtered surface seawater) and formalin preservative, a subsample of this initial brine in every tube was collected to determine initial [$bSiO_2$], [$Si(OH)_4$] and salinity. Tubes were deployed for 2 days at 60 m

and/or 100 m. After recovery, samples were filtered through a 200 μm filter. The >200 μm fraction was sorted microscopically to remove zooplankton before being recombined with <200 μm fraction. Aliquots from three different tubes were subsampled using a rotary splitter, to measure $bSiO_2$, and the filtrate was saved to measure silicic acid to determine the amount of $bSiO_2$ that dissolved during deployment [*Brzezinski et al.*, 2011] and to correct the total measured $bSiO_2$ flux. Sediment trap samples for particulate organic carbon and nitrogen (POC and PON) were similarly collected, fumed with HCl to drive off inorganic carbon, and analyzed on a CHN Analyzer at the Scripps Institution of Oceanography Analytical Facility. These data are used similarly to the primary and new production data, as an elemental basis of comparison to silicon.

3. Results

3.1. Defining the Frontal Region

Two 3 day experimental cycles were conducted in each of three water types: oceanic, frontal and coastal. During the cruise, the study area was affected by mesoscale eddies. The oceanic cycles appeared to be largely within an anticyclone (Figures 1a and 1d), while the two coastal cycles were conducted in or near cyclonic features (Figures 1b and 1c). The frontal cycles were located in the region between the two eddy types. A plot of temperature versus salinity (T-S) shows that the coastal and oceanic regions had distinctive T-S signatures (Figure 2a). The T-S signature at the frontal stations indicated mixing between the oceanic and coastal end members. This contrast was also observed in the vertical profiles of potential density, especially at depths below the surface mixed layer (e.g., >20 m, Figure 2b). The mixed layer depths, determined by potential density changes, in the oceanic cycles were deeper than for the coastal cycles, consistent with anticyclonic depression and cyclonic shoaling of isopycnals. The oceanic cycles in the anticyclone had a mixed-layer depth of 47±9 m, over twice the 20±9 m observed in the coastal cyclones (Table 1). The mixed-layer in the frontal region was 37±12 m. The potential density characteristics of frontal and coastal water overlapped in the upper 20 m (Figure 2b), but T-S relationships were more distinct and driven by changes in salinity (Figure 2a). Based on this observation, the oceanic, frontal and coastal water masses were operationally characterized by near-surface salinity that ranged from <33.15, 33.15–33.45, and >33.45, respectively.

3.2. C-Front Transect

The 23.3 km C-Front transect sampled a gradient between oceanic and coastal-cycle conditions. Using the near-surface salinity criteria, all three region types were sampled at least once on this transect (Figures 2c and 2d). After transitioning out of the oceanic region (0 km, i.e., transect starting station), the frontal water parcel (i.e., upper 40 m) was traversed in <9 km, with the remainder of the transect in coastal waters (Figure 3a). The frontal area of interaction between oceanic and coastal waters, per our salinity definition (triangles, Figures 2c and 2d), was observed between 3.8 and 9.1 km along the transect (Figure 3a). Surface waters between 9.0 and 19.5 km along the C-Front had higher potential density than waters to the east and west (Figure 3a). Within the upper 40 m, there was a strong uplift in the nitracline along the transect, as the 2.5 μM NO_3 isopleth shoaled from ~40 m in the oceanic water to ~20 m in the frontal water, and coastal-water nitrate exceeded 2.5 μM even at the surface (Figure 3b). In the frontal area, [$bSiO_2$] and [Chl a] were of similar magnitude to oceanic concentrations (Figure 3d); this may correlate with the silicic acid (Figure 3c), which was lower than nitrate in this water. Immediately in the coastal water (e.g., 9.0 km on the transect), [$bSiO_2$] increased by up to an order of magnitude relative to the front or offshore waters, ranging from 1.0 to nearly 4.0 μmol Si L^{-1} (Figure 3d), coincident with the increase in nitrate and silicic acid concentrations (Figures 3b and 3c). At the same stations and depths, [Chl a] ranged from 1.0 to >6.0 μg L^{-1} (Figure 3d). [$bSiO_2$] was spatially and vertically consistent with estimates of diatom carbon (Figure 3e), which increased to near 120 μg C L^{-1} in the high [$bSiO_2$] coastal waters compared to <20 μg C L^{-1} elsewhere. The close match in the vertical and spatial distribution of $bSiO_2$ and Chl a, suggests that diatoms dominated the autotrophic community biomass in coastal waters. This result is confirmed by the increase in diatom C to over 70% of the total phytoplankton biomass within these areas and depths, relative to <10% in the oceanic and frontal waters (Figure 3f).

3.3. Process Studies (Cycles)

All process stations were located within a relatively small area (~130 km x ~60 km) during the 30 day cruise (Figure 1). Drifter tracks were south to southeastward in five of six cycles (Figure 1), traveling at 29 – 66 cm s^{-1}, but were eastward at 17 cm s^{-1} during Cycle 3, inshore of the front. The fastest drift (66 cm s^{-1}) occurred during frontal Cycle 6 (Figure 1d).

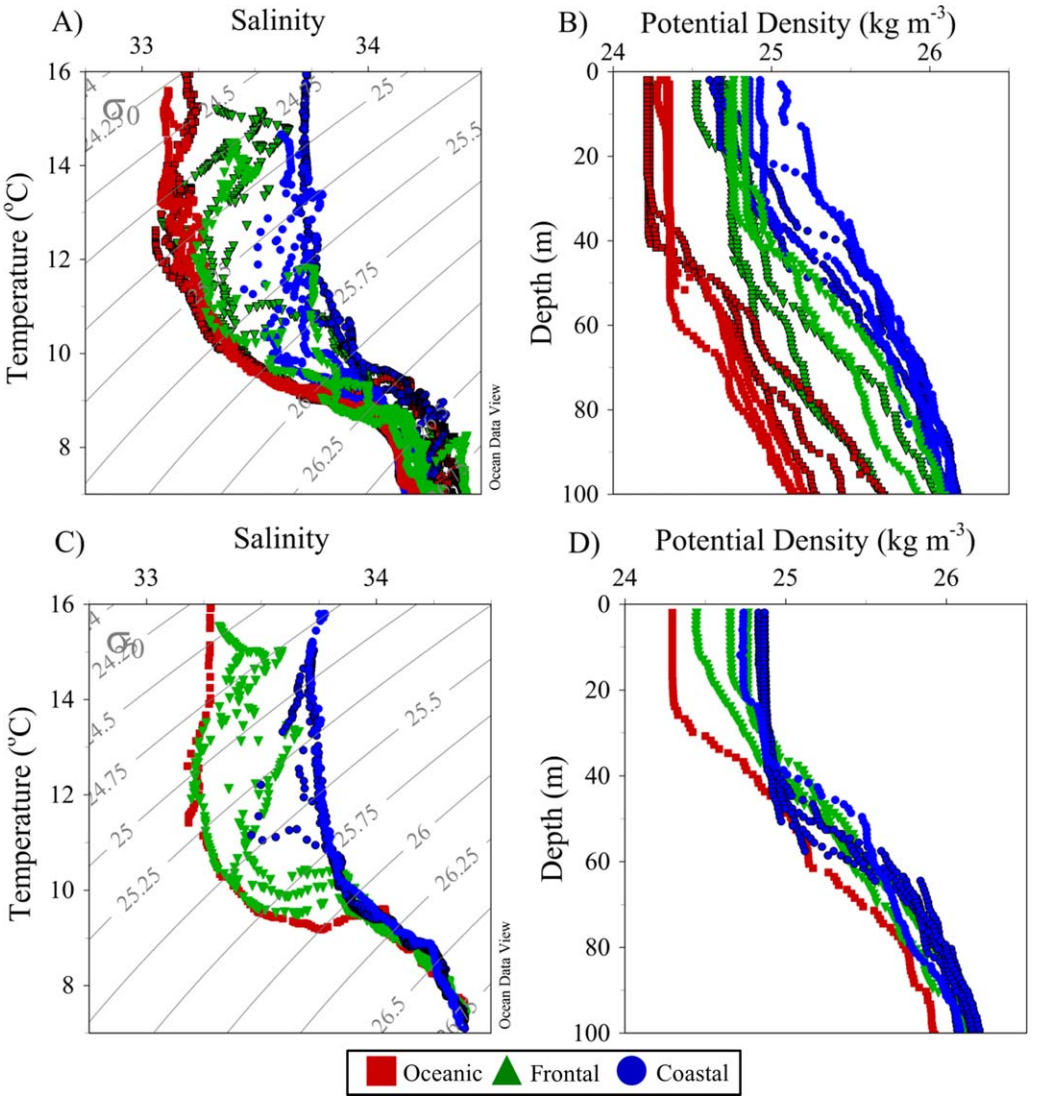

Figure 2. Hydrographic conditions during the (a, b) process studies and (c, d) C-Front transect. (a, c) Temperature versus Salinity (T-S) plots with potential density overlay (gray contours) and (b, d) Vertical profiles of potential density. Symbols: oceanic (red squares, Cycles 2 and 5), frontal (green triangles, Cycles 1, 6), and coastal (blue circles, Cycles 3 and 4). In Figures 2a and 2b, the black outlined symbols refer to Cycles 4–6; in Figures 2c and 2d, the black outlined symbol refer to the coastal profile not within the cyclonic eddy.

3.3.1. Nutrients

The horizontal and vertical trends in nitrate, silicic acid, and hydrography (supporting information Data Sets 1–3) were similar to those on the C-Front transect (Figure 3 and supporting information Data Set 4). Nitrate:-phosphate ratios (i.e., NO_3:PO_4) were <5 in the mixed layer, considerably lower than the canonical 16 (i.e., Redfield-Ketchum-Richards ratio). Thus, P limitation was unlikely, and P distributions will not be discussed further. In the mixed layer, nitrate and silicic acid showed opposing spatial trends (Figure 4). Nitrate was below detection limits in the oceanic regions (Figure 4a) but increased within the frontal (Figure 4c) and coastal regions (Figure 4c). Silicic acid concentrations at the frontal stations were slightly higher than those at oceanic stations (Figures 4a and 4b), but average concentrations at the coastal stations were considerably lower (Figure 4c). Profiles of silicic acid mirrored the differences in the mixed layer depth across location types (Figures 5a, 5e, and 5i) as the main silicic acid gradients were shallower in the frontal and coastal stations.

3.3.2. Biogenic Particles

Consistent spatial trends were observed in both biogenic silica and Chl *a* concentrations. Averaging the data for each cycle type (Figure 4), the mean mixed-layer [$bSiO_2$] was 0.04, 0.30 and 1.22 μmol Si L^{-1} for the oceanic, frontal, and coastal regions, respectively; however, there was significant variability in the coastal

Table 1. Biomass and Rates Across the Front[a]

Region (Cycle #)	Lat. (°N)	Long. (°W)	ML (m)	$\int bSiO_2$ (mmol Si m^{-2})	$\int \rho_P$ (mmol Si m^{-2} d^{-1})	V_{AVE} (d^{-1})	60 m ρ_E (mmol Si m^{-2} d^{-1})	60 m export Si:C (mol:mol)	60 m Export Si:N (mol:mol)	100 m ρ_E (mmol Si m^{-2} d^{-1})	100 m Export Si:C (mol:mol)	100 m Export Si:N (mol:mol)
Oceanic (2)	33.58	121.77	62	1.4	0.11	0.08	~	~	~	0.14±0.02	0.02	0.33
	33.42	121.62	52	1.4	0.12	0.08						
	33.22	121.47	46	1.3	~	~						
Oceanic (5)	33.38	121.41	35	2.1	0.15	0.07	~	~	~	0.25±0.03	0.03	0.40
	33.08	121.41	43	1.5	0.14	0.09						
	32.74	121.29	43	1.7	~	~						
Front (1)	34.04	121.70	28	9.1	2.47	0.15	4.01±0.07	0.22	1.66	5.62±0.39	0.85	8.80
	33.93	121.46	37	8.3	2.02	0.13						
	33.70	121.23	42	10.8	~	~						
Front (6)	33.52	121.11	18	3.4	1.10	0.28	4.30±0.22	0.18	1.79	2.01±0.13	0.10	1.10
	33.07	121.26	46	9.2	1.92	0.18						
	32.58	121.07	49	10.9	~	~						
Coast (3)	34.11	121.65	14	23.6	5.57	0.21	19.34±0.86	0.57	6.09	12.09±2.81	1.63	15.5
	34.06	121.47	36	11.9	1.74	0.20						
	34.10	121.42	22	18.7	~	~						
Coast (4)	33.53	121.09	10	91.7	3.35	0.03	4.69±0.16	0.28	2.80	3.95±0.19	0.78	7.65
	33.39	121.16	16	96.8	5.40	0.05						
	33.09	121.15	20	76.7	~	~						
Average (±SD)		Oceanic	47±9	1.6±0.3	0.13±0.02	0.08±0.01	~	~	~	0.19±0.08	0.03±<0.01	0.36±0.05
		Front	37±12	8.6±2.8	1.88±0.57	0.18±0.07	4.15±0.20	0.18	1.79	3.81±2.55	0.10	1.10
		Coast	20±9	53.2±39.3	4.01±1.82	0.12±0.09	12.01±10.36	0.42±0.20	4.45±2.33	8.02±5.76	1.20±0.61	11.58±5.56

[a]Vertical integrals are from 0 to 40 m, the mixed layer (ML) is based on 0.1 kg m^{-3} change in potential density from 5 m depth (consistent surface depth for all stations), and "~" indicates no data.

cycles. [$bSiO_2$] during coastal Cycle 3, the northern cyclone, averaged 0.23 μmol Si L^{-1}, but was 2.6 μmol Si L^{-1} during coastal Cycle 4, the southern cyclone (Figure 4c). This same increasing trend (0.12, 0.53 and 2.20 μg L^{-1}, respectively) was also evident for [Chl a] (Figure 4), as was the discrepancy between biomass during coastal Cycles 3 and 4. In vertical profiles, [Chl a] increased with depth to a subsurface maximum, and then rapidly attenuated (supporting information Data Set 1–3). In contrast, [$bSiO_2$] typically peaked in the mixed layer and declined with depth, with some exceptions (Figures 5b, 5f, and 5j). In the coastal waters, subsurface maxima between 25 and 35 m were observed during Cycle 4 (Figure 5j). The maximum values for both biomass measurements (i.e., $bSiO_2$ and Chl a) during Cycle 4 (coastal) were similar to those in the high-biomass region of the C-Front (Figures 3d, 4c, and 5h).

Integrating [$bSiO_2$] to 40 m depth amplified the differences between water types (Table 1). Average $\int bSiO_2$ was 53.2 mmol Si m^{-2} in the coastal regions, versus 8.6 and 1.6 mmol Si m^{-2} in the frontal and oceanic regions, respectively. Specifically, coastal Cycle 4 had a substantial $bSiO_2$ accumulation, which extended well below the mixed layer.

3.3.3. Biogenic Silica Production, Export, and Si Uptake Kinetics

The water-column distribution of biogenic silica production (ρ_P) paralleled that of [$bSiO_2$], with the highest ρ_P (Figures 5c, 5g,and 5k) at depths with highest biomass (Figures 5b, 5f, and 5g). ρ_P declined with depth to analytical zero values at the base of all profiles, i.e., 60–100 m (Figures 5c, 5g, and 5k), suggesting the profiles captured the full vertical extent of ρ_P. Unlike the biomass proxies, however, mixed-layer values of ρ_P in the coastal (0.069±0.031 μmol Si L^{-1} d^{-1}) and frontal regions (0.070±0.038 μmol Si L^{-1} d^{-1}) were nearly identical in magnitude and range (Figures 5g and 5k), and both were an order of magnitude higher than those in the oceanic region (Figure 5c). Two exceptions occurred in a single profile from both coastal Cycles 3 and 4, where the ρ_P maximum was observed below the mixed layer (~30 – 35 m, Figure 5k). The calculated biomass-normalized rates of production (V_b) (proxy for diatom growth rate) in the upper 20 m were highest in the frontal region (~0.2 – 0.3 d^{-1} in upper 20 m), compared to the oceanic (0.05 – 0.10 d^{-1}) and coastal (~ 0.05–0.2 d^{-1}) regions (Figures 5d, 5h, and 5l). By this estimation, the growth rate disparity between oceanic diatoms and those in coastal or frontal regions was not as large as suggested from the biomass measurements. When the rates are vertically integrated among regions to a common 40 m depth (typically deeper than the mixed layer in the coastal region), the subsurface maximum in ρ_P in the coastal region increased the integrated $\int \rho_P$ to nearly twice that observed in the frontal region (Table 1). However, depth-averaged values of V_b (i.e., V_{AVE}, Table 1) in the frontal region were still 50% higher than in the coastal

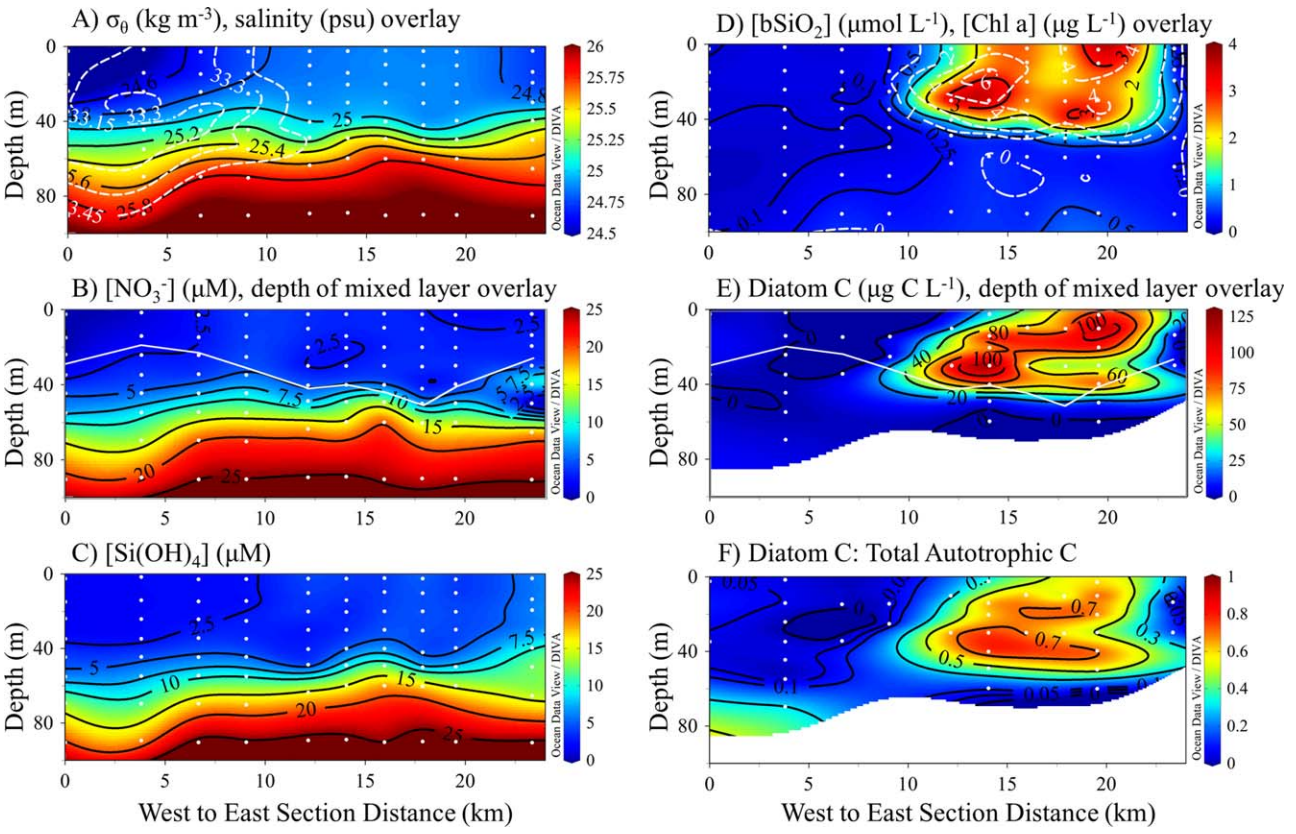

Figure 3. Section plots along the C-front transect. (a) Potential density with salinity overlay (white contours), (b) Dissolved nitrate with mixed layer depth overlay (white line), (c) Dissolved silicic acid (manual method), (d) Biogenic silica with Chlorophyll a overlay (white contours), (e) Diatom carbon with mixed layer depth overlay (white line), and (f) Proportion of diatom carbon to total autotrophic carbon.

region. These V_{AVE} values imply average doubling times of 3.9, 5.8, and 8.7 days for biogenic silica in the upper 40 m within the frontal, coastal and oceanic regions, respectively.

The export of $bSiO_2$ (ρ_E) to 60 and 100 m depth also showed strong spatial variability. One of the most surprising results was the enhanced ρ_E observed at coastal Cycle 3. ρ_E was 19.34 and 12.09 mmol Si m^{-2} d^{-1} at 60 and 100 m, respectively (Table 1), three to five-fold higher than ρ_E in the frontal region and Cycle 4 (coastal), which had the highest $\int bSiO_2$ (Table 1). Aside from the Cycle 3 values, measured export rates in the frontal and coastal waters were very similar, ~4.5 mmol Si m^{-2} d^{-1}.

Kinetic experiments show differences in Si uptake parameters across regions. V_{MAX} varied by a factor of 2.5 among experiments, with the highest and lowest values in the oceanic and frontal waters, respectively (Table 2). In the frontal and coastal regions, K_S concentrations were 0.63 and 1.17 μM, respectively (Table 2). Quasi-linear Si uptake was apparent in the oceanic experiment (Figure 6), as the r^2 for linear regression (i.e., 0.95) was the same as the adjusted r^2 when the data were fit to the Michaelis-Menten equation. Such linearity led to a calculated high K_S concentration (13.92±3.46 μM) relative to the available silicic acid. The average initial slope of the kinetic curve (V_{max}:K_s) was slightly higher in frontal versus coastal waters, and both diatom assemblages were more kinetically efficient for Si uptake than in the oceanic experiment. In all three regions, ambient silicic acid was low enough to limit rates of Si uptake (Figure 6). Silicic acid concentrations reduced uptake to 40.7%, 73.2% and 11.9% of V_{MAX} (i.e., V_b:V_{MAX}) for the coastal, frontal and oceanic communities, respectively (Table 2).

4. Discussion

4.1. Si-Cycling Across a Frontal Gradient

Rates of Si-cycling in the oceanic experimental cycles, both within an anticyclonic eddy, were consistent with previous studies in mid-ocean gyres. The gross rates of $bSiO_2$ production (ρ_P) were very low (Figure 5c and Table 1), similar to euphotic-zone rates at the Hawaii Ocean Time-series station ALOHA [*Brzezinski et al.*, 2011] and approximately 50–75% of summer-period rates in the North Pacific subtropical gyre near the

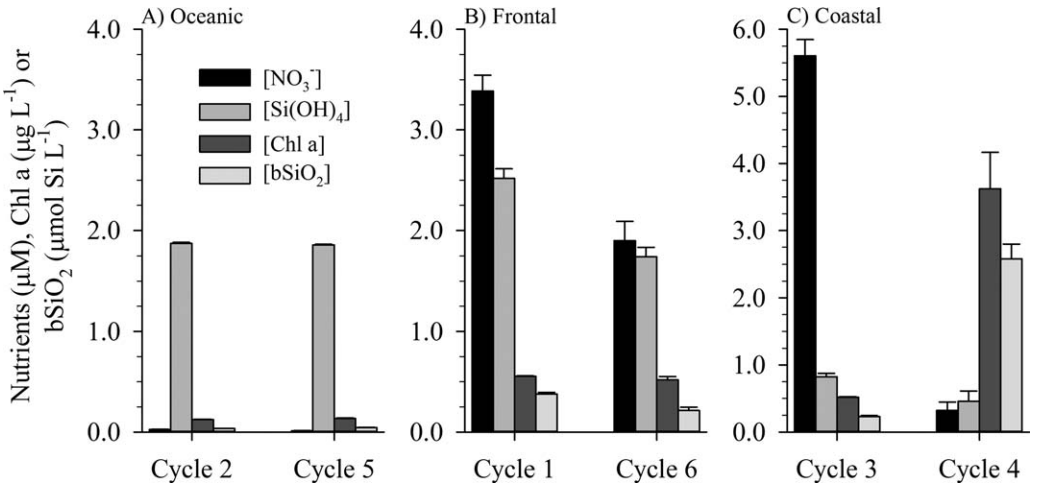

Figure 4. Comparison of mixed-layer nutrients (nitrate, silicic acid), Chlorophyll a and biogenic silica between cycles for (a) oceanic, (b) frontal, and (c) coastal zones (±SE). Note scale difference in Figure 4c.

subtropical front [*Krause et al*., 2013]. Despite the low ρ_P, V_b at the oceanic stations was higher than for coastal Cycle 4 (southern cyclonic eddy) but 33–50% of rates observed in the other three cycles (Figure 5), suggesting low and less-variable diatom growth in these waters. The quasi-linear increase with increasing silicic acid (Figure 6) clearly shows that diatom silicification was limited by available silicic acid, which held uptake rates to 11.9% of their maximum (Table 2). Limitation to such a degree may theoretically lead to diatom growth limitation from low silicic acid availability [*Martin-Jezequel et al*., 2000; *Krause et al*., 2012] despite the very low nitrate. Similar quasi-linear uptake responses to increasing silicic acid have also been observed in the mid-ocean gyres [*Brzezinski and Nelson*, 1996; *Brzezinski et al*., 1998; *Krause et al*., 2012] and in short-duration culture experiments [*Thamatrakoln and Hildebrand*, 2008]. However, this is the first report of this response in the CCE and one of the few reports of such a phenomenon occurring in such close proximity to the coast [see also *Brown et al*., 2003].

While diatom biomass and silica production rates increased between oceanic and coastal endpoints, the experiments within coastal waters showed considerable variability. At the time of sampling, diatoms in the southern cyclonic eddy (coastal Cycle 4) were likely in decline. The observed silicic acid in the mixed layer was 0.45±0.15 μM, with the surface values between 0.11 and 0.18 μM (Figure 4). Such intense silicic acid drawdown is seldom observed in the field and usually associated with intense coastal [e.g., *Nelson and Dortch*, 1996] or polar diatom blooms [e.g., *Brzezinski et al*., 2001]. Given the calculated kinetic parameters from both the frontal and coastal stations (Table 2), the low silicic acid concentrations in this coastal eddy likely led to severe limitation of Si uptake. Such limitation would reduce V_b to a low proportion of V_{MAX} (e.g., <20%), reducing ρ_P. Diatom biomass, by proxy of $bSiO_2$, was quite high in this eddy considering the offshore environment. Mean $\int bSiO_2$ during coastal Cycle 4 (cyclonic eddy) was similar to Monterey Bay during spring [*Brzezinski et al*., 2003] but on the low end observed in the Peru upwelling zone, where $\int bSiO_2$ ranged from 40–200 mmol Si m^{-2} during strong wind events, and 66–157 mmol Si m^{-2} under weak winds [*Nelson et al*., 1981]. *Nelson and Goering* [1978], working in the Baja California upwelling system, observed higher [$bSiO_2$] throughout the euphotic zone (e.g., ~0.5–9.0 μmol Si L^{-1}). Thus, diatom biomass observed in the coastal Cycle 4 (cyclonic eddy) was on the lower end of that observed in other near-shore eastern-boundary upwelling systems. While biomass was elevated, the highest $\int \rho_P$ observed in this study (i.e., coastal cycles) was an order of magnitude lower than observed during spring in Monterey Bay [*Brzezinski et al*., 2003]. The highest maximum specific uptake rates (Figures 5h and 5l) were ~five-fold lower than rates observed in Baja and Peru [*Nelson and Goering*, 1978; *Nelson et al*., 1981].

These comparisons underscore that this particular offshore region of the CCE is highly dynamic over relatively short spatial scales (e.g., <40 km). $\int bSiO_2$ and $\int \rho_P$ vary from low values similar to subtropical gyres [*Brzezinski et al*., 2011; *Krause et al*., 2013] and high values within the low range observed in eastern-boundary coastal upwelling systems. Such a range spans a high proportion of the entire Pacific basin-scale

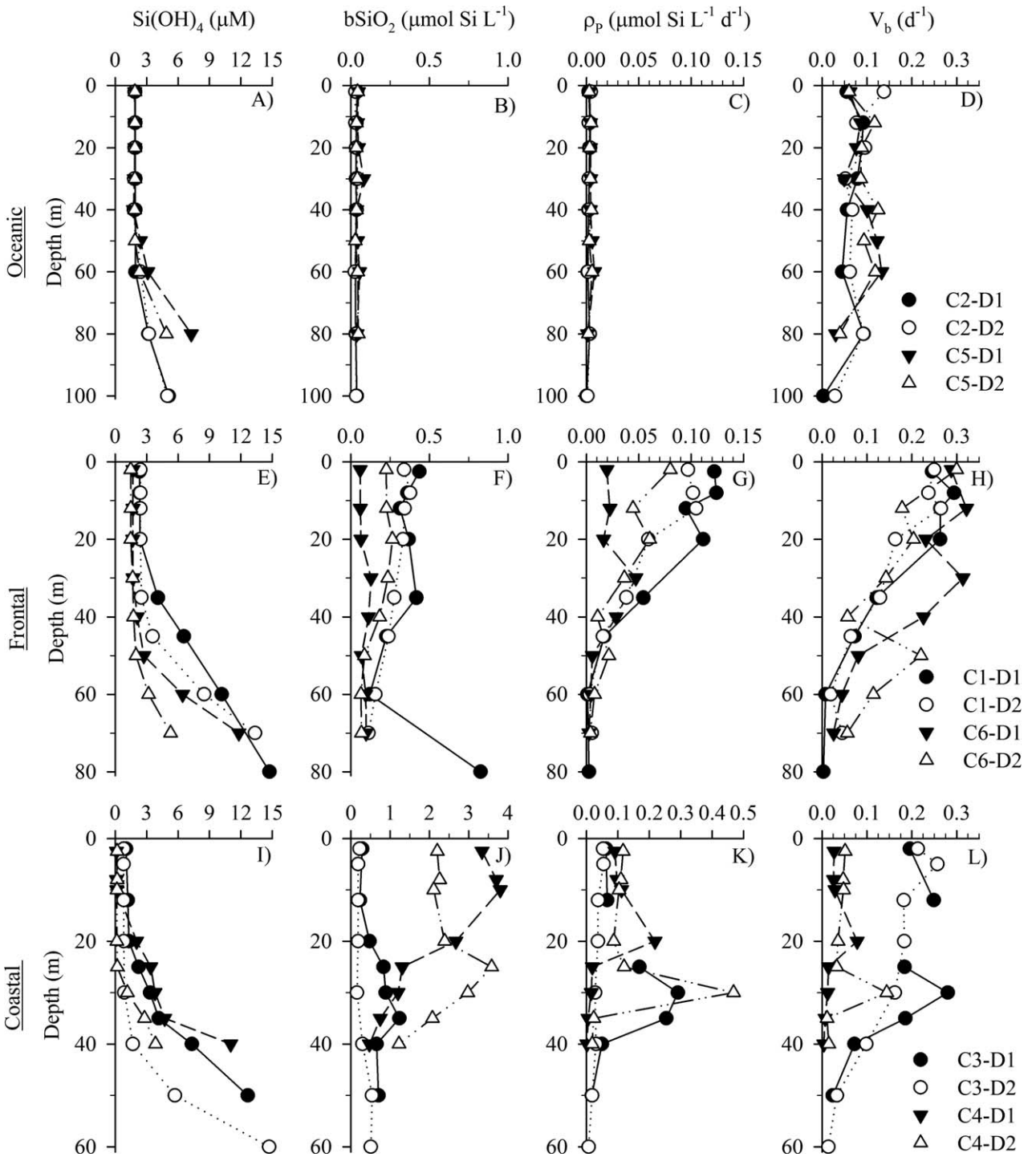

Figure 5. Vertical profiles of (a, e, i) dissolved silicic acid, (b, f, j) biogenic silica, and (c, g, k) gross biogenic silica production and (d, h, l) biomass-specific biogenic silica production for the (a–d) oceanic, (f–h) frontal, and (i–l) coastal regions (bars ±SE). Legend for symbols per region denotes the cycle number (e.g., Cycle 1 = C1) and the day (e.g., Day 1 = D1) of the hydrocast during a specific cycle. Note scale differences in Figures 5j and 5k for the coastal cycles.

of variability for these measurements. If the variability observed in biomass during C-Front is representative for rates, the spatial scale for this variability may be even shorter (e.g., <10 km, Figure 3).

Two lines of evidence support that the coastal Cycle 4 bloom was in decline. First, the V_b observed in both the coastal Cycle 3 and frontal cycles were approximately twice that of coastal Cycle 4 (Figure 5). This could reflect limitation by the low ambient [$Si(OH)_4$] or the presence of a higher fraction of detrital $bSiO_2$ [*Krause*

Table 2. Kinetic Parameters From Single Experiments Conducted in Each Type of Region[a]

Region (Cycle #)	Lat. (°N)	Long. (°W)	$[Si(OH)_4]$ (μM)	V_b (h^{-1})	V_{MAX} (h^{-1})	K_S (μM)	V_{MAX}:K_S (mmol L^{-1} $h)^{-1}$	V_b:V_{MAX} (%)
Oceanic (2)	33.22	121.47	1.87	0.003	0.025 ±0.004	13.92 ±3.46	1.8 ± 0.5	11.9 ±2.3
Front (6)	32.58	121.07	1.73	0.007	0.010 ±0.001	0.63 ±0.31	15.5± 7.5	73.2 ±6.3
Coast (3)	34.10	121.42	0.81	0.006	0.015 ±0.001	1.17 ±0.31	13.1 ± 3.5	40.7 ±3.0

[a]V_{MAX}:K_S is a proxy for nutrient-use efficiency at low $[Si(OH)_4]$ [*Healey*, 1980] and V_b:V_{MAX} expresses the percentage of maximum Si uptake supported by dissolved silicic acid observed or normalized to a constant dissolved silicic acid. Standard error was calculated for V_{MAX} and K_S based on the nonlinear curve fitting analysis, and error estimates for V_{MAX}:K_S, V:V_{MAX} were propagated assuming that V_b and V_{MAX} had the same standard error.

et al., 2010a], as both are indicative of a declining diatom bloom. Second, given the weakening of this cyclonic eddy in the two weeks prior to Cycle 4 sampling (i.e., Figures 1a–1c), the isopycnal uplift and subsequent nutrient entrainment into the euphotic zone were likely reduced. Such a weakening may also have helped accelerate the silicic acid drawdown, which lowered surface concentrations to ~0.1 μM, by limiting the input rate of silicic acid from depth.

Coastal Cycle 3 was conducted on the edge of the northern cyclonic eddy (Figure 1b), and the observations suggest the diatom community within this feature was limited by iron. Low dissolved iron concentrations were measured throughout the cruise [*Bundy,* 2014]. Within the mixed layer, the ratio of silicic acid to nitrate (Si:N) averaged 0.15±0.01 (SE) during Cycle 3, as opposed to 2.2±0.6 for the same vertical interval during Cycle 4 (Figure 4). Diatoms typically require Si in near equal amounts to N (i.e., Si:N 1:1) and ~seven-fold less than C (i.e., Si:C 0.13) [*Brzezinski*, 1985]. When diatom growth is limited by iron, the period of the cell cycle where Si uptake occurs increases, thereby increasing the Si:N and Si:C uptake ratios integrated over a division cycle even when Si is kinetically limiting [*Hutchins and Bruland*, 1998; *Takeda*, 1998; *Franck et al*., 2000]. The low Si:N, driven by intense silicic acid drawdown, therefore provides an indirect indication of iron limitation of diatom growth. Additionally, under iron limitation, the Si:N and Si:C ratios of exported material are expected to increase, reflecting the changes in diatom physiology. The total $bSiO_2$ export during coastal Cycle 3 was over three-fold higher than export measured in coastal Cycle 4 and both frontal cycles (Table 1). The exported material was also enriched in Si, relative to N (Si:N ~8–15) and C (Si:C ~0.8–1.6), and this enrichment was higher than would be expected from differential remineralization between $bSiO_2$ and organic matter, e.g., as observed for the 60 m samples in the frontal cycles and coastal Cycle 4 (Table 1). Thus, by two independent and indirect metrics, diatoms in coastal Cycle 3 appeared to be growth limited by iron. This result is consistent with previous reports of iron-limitation of the phytoplankton community in the California Current region [*Bruland et al*., 2001; *King and Barbeau*, 2007].

Despite a lack of biomass accumulation, diatom activity in frontal waters (Cycles 1, 6) appeared to be enhanced. V_b in the frontal waters was high compared to the coastal eddies (Cycles 3, 4; Table 1). The physical interaction within these frontal regions increased silicic acid concentrations in the mixed layer (Figure 4b) by a factor of three compared to the coastal eddy cycles (Figure 4c) and ~15% above those in the oceanic eddy cycles (Figure 4a). That increase in Si availability combined with the high affinity of the frontal assemblage for silicic acid (i.e., high V_{MAX}:K_S) [*Healey*, 1980] would boost cell division and hence biomass normalized production, V_b.

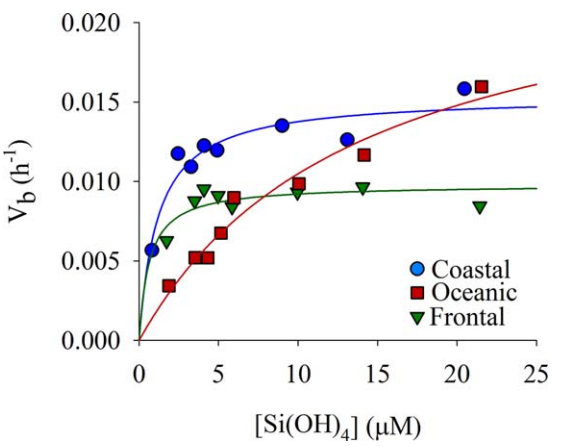

Figure 6. Response of Si uptake to enhanced dissolved silicic acid availability. One experiment was conducted in each region (symbols). Data were fit to the Michaelis-Menten equation using a nonlinear regression analysis in Sigma Plot 12.0 © software.

4.2. Diatom Biomass Along the C-Front Transect

Diatom biomass at the C-Front was enhanced, but this did not appear to result from local frontal processes. Satellite-derived sea-surface height anomalies (Figure 1), potential density profiles (Figure 2), and diatom biomass observed during the process studies (Figures 4

Table 3. The Diatom Contribution to Primary and New Production and Organic-Matter Export[a]

	$\int$PP (mmol C m^{-2} d^{-1})		$\int \rho NO_3^-$ (mmol NO_3^- m^{-2} d^{-1})		ρ_{POC} export (mmol C m^{-2} d^{-1})		ρ_{PON} export (mmol N m^{-2} d^{-1})	
Region (Cycle)	Rate	%Diatom	Rate	%Diatom	Rate	%Diatom	Rate	%Diatom
Oceanic (2)	15.0 ±1.5	8% ±<1%	0.3±0.3[b]	7% ± <1%	8.4	0.5%	0.6	1.0%
Oceanic (5)	14.3 ±2.2	6% ±1%	0.7±0.2[b]	5% ± 1%	5.8	0.4%	0.4	0.8%
Frontal (1)	59.3 ±20.5	30% ±6%	4.6±1.8	26% ± 5%	18.2	7%	2.4	8%
Frontal (6)	51.9 ±11.2	22% ±4%	2.4±0.8	19% ± 3%	23.5	6%	2.4	8%
Coastal (3)	78.4 ±6.94	37% ±30%	5.6±1.8	32% ± 26%	34.1	44%	3.2	72%
Coastal (4)	81.4 ±11.0	43% ±20%	2.8±2.3	37% ± 17%	16.7	22%	1.7	33%

[a]See text for calculations. For the coastal and front regions, POC and PON export rates at 60 m are used and 100 m export values are used for the oceanic region.
[b]Value likely biased high due to low ambient nitrate and potential for adding too much stable isotope tracer.

and 5) suggest the C-Front transect traversed part of the southern cyclonic eddy (i.e., sampled during Cycle 4). Thus, the elevated diatom biomass was not from frontal dynamics as observed previously in the southern CCE [e.g., *Taylor et al*., 2012] but likely the result of advection.

4.3. Diatom Contribution to Primary Production and Export Production Across Frontal Gradients

The contribution of diatoms to primary production and export production across the frontal gradients can be estimated from the rates of C, N and Si use and particle elemental ratios. Si, C and N uptake rates are coupled to estimate the contributions of diatoms to primary production (PP) and nitrate uptake (i.e., new production, ρNO_3^-) as follows:

$$\text{Diatom } \% \int \text{PP} = 100 \times \int \rho_P \Big/ \left[(\text{Si} : \text{C}) \times \left(\int \text{PP} \right) \right] \tag{2}$$

$$\text{Diatom } \% \int \rho NO_3^- = \left\{ 100 \times \int \rho_P \Big/ \left[(\text{Si} : \text{N}) \times \left(\int \rho NO_3^- \right) \right] \right\} \times f\text{-ratio} \tag{3}$$

$$f\text{-ratio} = \left(\int \rho NO_3^- \times \text{ C} : \text{N} \right) \Big/ \int \text{PP} \tag{4}$$

Culture-based diatom Si:C and Si:N values of 0.13 and 1.0, respectively, are used [*Brzezinski*, 1985] and a 6.6 C:N ratio is assumed.

Estimates of the diatom contributions to primary and new production both indicate an important biogeochemical footprint for diatoms in this system. In the coastal cycles (3, 4), diatoms potentially account for ~40% of primary production. Considering the role of diatoms in near-shore coastal systems, especially during episodic nutrient pulses, these results in offshore coastal waters are not unexpected and fit with previous studies in the CCE (e.g., northern region) [*Lassiter et al*., 2006].

Diatoms were also important in the oceanic cycles (2, 5). On the C-Front transect, diatom biomass was typically ~5% of the total autotrophic biomass in the oceanic region (i.e., Diatom C: Total Autotrophic C, Figure 3f). If this proportion is conserved, then the importance of diatoms to primary production in the oceanic cycles (~7%, Table 3) is similar to or slightly higher than their contribution to autotrophic biomass. Such a result fits well with many studies from the open-ocean including the subtropical gyres [*Nelson and Brzezinski*, 1997; *Brzezinski et al*., 2011] and the equatorial Pacific [*Krause et al*., 2011b]. Each of these studies demonstrate similar disproportionate importance of diatoms in primary production relative to their low biomass, suggesting that diatoms play quantitatively significant roles in biogeochemical cycling outside of near-shore coastal and high-latitude systems.

Within the frontal region, diatom contributions to community rates resembled a blend of the oceanic and coastal cycle estimations. In the frontal areas (Cycles 1, 6), diatoms accounted for ~25% of total primary production. Despite the five-fold decrease in diatom biomass (Table 1, Figure 5), the diatom contribution to PP was approximately half of the contribution in coastal waters, indicating a quantitatively significant role for diatoms in community rates at these locations.

Similarly, diatoms appear to be disproportionately important contributors to new production relative to their biomass. In the coastal cyclones (Cycles 3, 4), diatoms accounted for ~35% of nitrate uptake (Table 3).

While nitrate concentrations were sufficiently low in the oceanic domain (Cycles 2, 5; Figure 4a) to positively bias ^{15}N uptake measurements, the calculated contribution for diatoms was ~6%, which is consistent with the estimated diatom proportion of primary production (Table 3). Estimates of nitrate uptake by diatoms at the frontal stations (Cycles 1, 6) closely resembled those for primary production in both magnitude and range (19–26%, Table 3), suggesting that the frontal diatom communities also played a quantitatively significant role in new production.

Two lines of evidence indicate that the estimates of diatom new production may be conservative, especially in the frontal region. First, *Dugdale and Wilkerson* [1989] reported *f*-ratios between 0.6 and 0.8 in the upper euphotic zone during a 5 day drifter experiment with coastal water originating near Pt. Conception, slightly north and in shore of our study region. *Dugdale et al*. [2007] also reported that >5 μm cells in near-surface waters of the eastern equatorial Pacific typically had *f*-ratios of 0.6. These studies demonstrated that larger cells, e.g., diatoms, may use proportionally more nitrate than reduced N for production of organic matter. Thus, applying a community *f*-ratio (i.e., as in Table 3) artificially reduces the estimates of diatom contributions to new production in the frontal and coastal areas. Second, *Harrison et al*. [1987] determined a regression for predicting *f*-ratio values from $[NO_3]$:$[NO_3+NH_4]$ concentration ratios for the Southern California Bight (regional data originally from *Eppley et al*. [1979]). From this regression, nutrient ratios in the upper 40 m (i.e., the depth of production integrations) during our cruise would predict *f*-ratios of 0.22, 0.60 and 0.44, for oceanic, frontal and coastal stations, respectively. Compared to the *f*-ratios used for calculations in Table 3 (0.23, 0.40 and 0.35 for the oceanic, frontal and coastal regions, respectively), the *Harrison et al*. [1987] regression predicts a disproportionately higher *f*-ratio in the front region. Considering these previous studies, the estimated contribution of diatoms to new production at the frontal stations may be up to 1.5-fold higher than suggested in Table 3 (i.e., real *f*-ratio for diatoms may have been near 0.6 in the front). This would revise the estimated nitrate uptake to values similar to the coastal region.

For estimating the contribution of diatoms to POC and PON export, our calculation approach is similar to equations (2) and (3):

$$\text{Diatom \%POC or \%PON export} = \{100 \times \rho_E / [(\text{Si : C or Si : N}) \times (\rho_{POC} \text{ or } \rho_{PON})]\} \quad (5)$$

Previous reports that estimate the diatom contribution to organic matter export use nutrient-replete diatom Si:C and Si:N ratios which are modified due to recycling of organic carbon and $bSiO_2$ within the euphotic zone [e.g., *Brzezinski et al*., 2011]. In this study, neither recycling term is well constrained nor is it known whether diatoms sink as whole cells, thus exporting all their organic material to the trap. The potential export pathways for diatom material out of the euphotic zone include sinking as an intact cell, within a zooplankton fecal pellet, or incorporated into an aggregate. If diatom detrital material gets consumed more than once, e.g., mesozooplankton grazing on fecal pellets or detrital aggregates, then the resulting diatom Si:C increases and the actual export of diatom organic matter is reduced. The most important pathway above cannot be determined with the current data set. Thus, instead of using modified diatom Si:C and Si:N based on nutrient-replete diatoms, we use Si:C based on the ratio of $bSiO_2$:diatom C for the oceanic, frontal and coastal conditions, 6.1±2.3, 3.2±0.9, and 1.3±0.5, respectively (data from Figures 3d and 3e). This approach assumes diatom particulate material in the euphotic zone is well mixed from grazing, aggregation and disaggregation, and that the likelihood to sink, be grazed, and be incorporated into aggregates is similar for living diatoms and empty frustules (i.e., detritus).

While methodological bias in the collection of exported material would increase the uncertainty of the diatom contribution to organic matter export, this does not appear to have been an issue during this cruise. Combined use of ^{234}Th:^{238}U disequilibrium and identical sediment trap arrays to those used in this study have shown good agreement for carbon fluxes in the CCE [*Stukel et al*., 2013], suggesting that our bulk export results are unlikely to suffer from significant over or under-collection.

The variability in the contribution of diatoms to organic matter export across the front is a striking feature of our results. In the coastal cyclones, diatoms alone could account for 22–44% and 33–72% of POC and PON export, respectively (Table 3). The high values in the coastal cycles are not surprising given that the importance of diatoms to particle export in coastal systems is well established. The higher values were from Cycle 3, where iron limitation of diatom growth was suggested. Such a condition would result in heavily silicified diatoms, which sink faster than iron-replete diatoms, with relatively low organic matter content. In

the oceanic waters, the diatom contribution to organic-matter export was considerably lower ($\leq$1%) than their maximum contribution to primary and new production (Table 3). This suggests that most of the produced diatom organic matter was either remineralized in the euphotic zone or assimilated by higher trophic organisms, rather than exported as intact single cells or aggregates. In the frontal area, diatoms could account for 6–8% of export, relative to POC or PON proxies (Table 3), an order-of-magnitude enhancement in proportional importance compared to the oceanic region. Despite the similarity in the gross rates of $bSiO_2$ export between the frontal cycles (1, 6) and coastal Cycle 4, where diatoms were not iron limited, the diatom contribution to organic matter export was approximately four-fold lower in the front than in the coastal region. Such a difference implies there was considerable reworking of diatom organic matter in the frontal-region food web prior to export. When considering all three water types, the food web processes which transform diatom material prior to export appear to be highly variable on short spatial scales.

5. Conclusion

Even with a 25-fold variability in diatom biomass across a frontal zone in the CCE, the biogeochemical roles of diatoms were significant in each of three water types studied. Oceanic diatoms had low biomass and production rates, but their contributions to organic matter production was higher than their contribution to autotrophic biomass and most of diatom organic matter was retained in the food web. Diatom biomass and rates of biogenic silica production were highly variable within two coastal cyclonic eddies, but in both their contribution to organic matter export was high. Despite frontal diatom biomass being $\sim$20% of the coastal cyclones, diatom $bSiO_2$ export was similar and their contribution to organic matter export was four-fold lower, suggesting a stronger importance for food web processes in retaining diatom organic matter in the euphotic zone. Convergent fronts may retain buoyant particles which ultimately may lead to elevated export despite the strong likelihood that most of the biomass was not produced at the front [*Yoder et al*., 1994]. The interactions between eddies, which presumably created the frontal zone, appear to be the physical mechanism that created variability over $<$40 km spatial scale comparable to that previously observed across the Pacific basin. This mesoscale-scale variability across the front is expressed in diatom biomass, production rates, and food web processes that transform diatom material prior to export. If the biomass variability from the C-Front transect is also representative of rate variability, this spatial scale may be shorter, e.g., $<$10 km. This result differs from other fronts examined in this region [e.g., *Landry et al*., 2012*, Ohman et al*., 2012] and suggests eddy-eddy interactions may play an important role in driving high spatial variability in biogeochemical rates across frontal zones in the southern CCE.

Acknowledgments
The primary data for this paper are available through CCE LTER data archive at http://oceaninformatics.ucsd.edu/datazoo/ or from the author upon request; altimeter products were distributed by Aviso (http://www.aviso.oceanobs.com). This work was supported by the California Current Ecosystem Long Term Ecological Research program under award OCE 1026607 (awarded to MDO, MRL, RG) by the National Science Foundation. This manuscript benefitted from comments by K. Barbeau and P. Franks. We thank the science party and crew of the R/V Melville for their support and technical assistance, specifically A. De Verneil, D. Faber, and J. Wokuluk, and logistical support at UCSB by J. Jones and L. Windecker.

References

Alldredge, A. L., and C. Gotschalk (1988), In situ settling behavior of marine snow, *Limnol. Oceanogr.*, *33*(3), 339–351.
Benitez-Nelson, C. R., et al. (2007), Mesoscale eddies drive increased silica export in the subtropical Pacific Ocean, *Science*, *316*(5827), 1017–1021, doi:10.1126/science.1136221.
Brown, L., R. Sanders, G. Savidge, and C. H. Lucas (2003), The uptake of silica during the spring bloom in the Northeast Atlantic Ocean, *Limnol. Oceanogr. Methods*, *48*(5), 1831–1845.
Bruland, K. W., E. L. Rue, and G. J. Smith (2001), Iron and macronutrients in California coastal upwelling regimes: Implications for diatom blooms, *Limnol. Oceanogr.*, *46*(7), 1661–1674.
Brzezinski, M. A. (1985), The Si:C:N ratio of marine diatoms: Interspecific variability and the effect of some environmental variables, *J. Phycol.*, *21*(3), 347–357.
Brzezinski, M. A., and D. M. Nelson (1995), The annual silica cycle in the Sargasso Sea near Bermuda, *Deep Sea Res., Part I*, *42*(7), 1215–1237.
Brzezinski, M. A., and D. M. Nelson (1996), Chronic substrate limitation of silicic acid uptake rates in the western Sargasso Sea, *Deep Sea Res., Part II*, *43*(2-3), 437–453.
Brzezinski, M. A., and D. R. Phillips (1997), Evaluation of Si-32 as a tracer for measuring silica production rates in marine waters, *Limnol. Oceanogr.*, *42*(5), 856–865.
Brzezinski, M. A., T. A. Villareal, and F. Lipschultz (1998), Silica production and the contribution of diatoms to new and primary production in the central North Pacific, *Mar. Ecol. Prog. Ser.*, *167*, 89–104.
Brzezinski, M. A., D. M. Nelson, V. M. Franck, and D. E. Sigmon (2001), Silicon dynamics within an intense open-ocean diatom bloom in the Pacific sector of the Southern Ocean, *Deep Sea Res., Part II*, *48*(19-20), 3997–4018.
Brzezinski, M. A., J. L. Jones, K. D. Bidle, and F. Azam (2003), The balance between silica production and silica dissolution in the sea: Insights from Monterey Bay, California, applied to the global data set, *Limnol. Oceanogr. Methods*, *48*(5), 1846–1854.
Brzezinski, M. A., J. W. Krause, M. J. Church, D. M. Karl, B. Li, J. L. Jones, and B. Updyke (2011), The annual silica cycle of the North Pacific subtropical gyre, *Deep Sea Res., Part I*, *58*(10), 988–1001, doi:10.1016/j.dsr.2011.08.001.
Bundy, R. M. (2014), Iron and copper organic complexation in marine systems: Detection of multiple ligand classes via electrochemistry, PhD dissertation, 250 p., Univ. of Calif., San Diego, Calif.
Dugdale, R. C., and F. P. Wilkerson (1989), New production in the upwelling center at Point Conception, California: Temporal and spatial patterns, *Deep Sea Res., Part A*, *36*(7), 985–1007, doi:10.1016/0198-0149(89)90074-5.

Dugdale, R. C., F. P. Wilkerson, F. Chai, and R. Feely (2007), Size-fractionated nitrogen uptake measurements in the equatorial Pacific and confirmation of the low Si-high-nitrate low-chlorophyll condition, *Global Biogeochem. Cycles*, *21*, 10, GB2005, doi:10.1029/2006GB002722.

Eppley, R., E. Renger, and W. Harrison (1979), Nitrate and phytoplankton production in southern California coastal waters, *Limnol. Oceanogr.*, *24*(3), 483–494.

Franck, V. M., M. A. Brzezinski, K. H. Coale, and D. M. Nelson (2000), Iron and silicic acid concentrations regulate Si uptake north and south of the Polar Frontal Zone in the Pacific Sector of the Southern Ocean, *Deep Sea Res., Part II*, *47*(15-16), 3315–3338.

Harrison, W., T. Platt, and M. R. Lewis (1987), *f*-Ratio and its relationship to ambient nitrate concentration in coastal waters, *J. Plankton Res.*, *9*(1), 235–248.

Healey, F. P. (1980), Slope of the Monod equation as an indicator of advantage in nutrient competition, *Microbial Ecol.*, *5*(4), 281–286.

Hutchins, D. A., and K. W. Bruland (1998), Iron-limited diatom growth and Si:N uptake ratios in a coastal upwelling regime, *Nature*, *393*(6685), 561–564.

Kahru, M., E. Di Lorenzo, M. Manzano-Sarabia, and B. G. Mitchell (2012), Spatial and temporal statistics of sea surface temperature and chlorophyll fronts in the California Current, *J. Plankton Res.*, *34*(9), 749–760.

King, A. L., and K. Barbeau (2007), Evidence for phytoplankton iron limitation in the southern California Current System, *Mar. Ecol. Prog. Ser.*, *342*, 91–103.

Koslow, J., R. Goericke, A. Lara-Lopez, and W. Watson (2011), Impact of declining intermediate-water oxygen on deepwater fishes in the California Current, *Mar. Ecol. Prog. Ser.*, *436*, 207–218.

Krause, J. W., M. W. Lomas, and D. M. Nelson (2009a), Biogenic silica at the Bermuda Atlantic Time-series Study site in the Sargasso Sea: Temporal changes and their inferred controls based on a 15-year record, *Global Biogeochem. Cycles*, *23*, GB3004, doi:10.1029/2008GB003236.

Krause, J. W., D. M. Nelson, and M. W. Lomas (2009b), Biogeochemical responses to late-winter storms in the Sargasso Sea, II: Increased rates of biogenic silica production and export, *Deep Sea Res., Part I*, *56*(6), 861–874, doi:10.1016/j.dsr.2009.01.002.

Krause, J. W., M. A. Brzezinski, M. R. Landry, S. B. Baines, D. M. Nelson, K. E. Selph, A. G. Taylor, and B. S. Twining (2010a), The effects of biogenic silica detritus, zooplankton grazing, and diatom size structure on silicon cycling in the euphotic zone of the eastern equatorial Pacific, *Limnol. Oceanogr. Methods*, *55*(6), 2608–2622, doi:10.4319/lo2010.55.6.2608.

Krause, J. W., D. M. Nelson, and M. W. Lomas (2010b), Production, dissolution, accumulation and potential export of biogenic silica in a Sargasso Sea mode-water eddy, *Limnol. Oceanogr. Methods*, *55*(2), 569–579, doi:10.4319/lo.2010.55.2.0569.

Krause, J. W., M. A. Brzezinski, and J. L. Jones (2011a), Application of low level beta counting of 32Si for the measurement of silica production rates in aquatic environments, *Mar. Chem.*, *127*, 40–47, doi:10.1016/j.marchem.2011.07.001.

Krause, J. W., D. M. Nelson, and M. A. Brzezinski (2011b), Biogenic silica production and the diatom contribution to primary production and nitrate uptake in the eastern equatorial Pacific Ocean, *Deep Sea Res., Part II*, *58*(3-4), 434–448, doi:10.1016/j.dsr2.2010.08.010.

Krause, J. W., M. A. Brzezinski, T. A. Villareal, and C. Wilson (2012), Increased kinetic efficiency for silicic acid uptake as a driver of summer diatom blooms in the North Pacific Subtropical Gyre, *Limnol. Oceanogr. Methods*, *57*(4), 1084–1098, doi:10.4319/lo.2012.57.4.1084.

Krause, J. W., M. A. Brzezinski, T. A. Villareal, and C. Wilson (2013), Biogenic silica cycling during summer phytoplankton blooms in the North Pacific subtropical gyre, *Deep Sea Res., Part I*, *71*, 49–60, doi:10.1016/j.dsr.2012.09.002.

Landry, M. R., M. D. Ohman, R. Goericke, M. R. Stukel, and K. Tsyrklevich (2009), Lagrangian studies of phytoplankton growth and grazing relationships in a coastal upwelling ecosystem off Southern California, *Prog. Oceanogr.*, *83*(1), 208–216.

Landry, M. R., M. D. Ohman, R. Goericke, M. R. Stukel, K. A. Barbeau, R. Bundy, and M. Kahru (2012), Pelagic community responses to a deep-water front in the California Current Ecosystem: Overview of the A-Front Study, *J. Plankton Res. 34*, 739–748.

Lara-Lopez, A. L., P. Davison, and J. A. Koslow (2012), Abundance and community composition of micronekton across a front off Southern California, *J. Plankton Res. 34*, 828–848.

Lassiter, A. M., F. P. Wilkerson, R. C. Dugdale, and V. E. Hogue (2006), Phytoplankton assemblages in the CoOP-WEST coastal upwelling area, *Deep Sea Res., Part II*, *53*(25-26), 3063–3077.

Li, Q. P., P. J. Franks, M. D. Ohman, and M. R. Landry (2012), Enhanced nitrate fluxes and biological processes at a frontal zone in the southern California current system, *J. Plankton Res. 34*, 790–801.

Martin-Jezequel, V., M. Hildebrand, and M. A. Brzezinski (2000), Silicon metabolism in diatoms: Implications for growth, *J. Phycol.*, *36*(5), 821–840.

McGillicuddy, D. J., et al. (2007), Eddy/wind interactions stimulate extraordinary mid-ocean plankton blooms, *Science*, *316*(5827), 1021–1026.

Nelson, D. M., and M. A. Brzezinski (1997), Diatom growth and productivity in an oligotrophic midocean gyre: A 3-yr record from the Sargasso Sea near Bermuda, *Limnol. Oceanogr.*, *42*(3), 473–486.

Nelson, D. M., and Q. Dortch (1996), Silicic acid depletion and silicon limitation in the plume of the Mississippi River: Evidence from kinetic studies in spring and summer, *Mar. Ecol. Prog. Ser.*, *136*(1-3), 163–178.

Nelson, D. M., and J. J. Goering (1978), Assimilation of silicic acid by phytoplnakton in the Baja California and Northwest Africa upwelling systems, *Limnol. Oceanogr.*, *23*(3), 508–517.

Nelson, D. M., J. J. Goering, and D. W. Boisseau (1981), Consumption and regeneration of silicic acid in three coastal upwelling systems, in *Coastal Upwelling*, edited by F. A. Richards, pp. 242–256, AGU, Washington, D. C.

Nelson, D. M., et al. (1985), Distribution and composition of biogenic particulate matter in a Gulf Stream warm-core ring, *Deep Sea Res., Part A*, *32*, 1347–1369.

Ohman, M. D., J. R. Powell, M. Picheral, and D. W. Jensen (2012), Mesozooplankton and particulate matter responses to a deep-water frontal system in the southern California Current System, *J.Plankton Res.*, *34*(9), 815–827.

Ohman, M. D., K. Barbeau, P. J. Franks, R. Goericke, M. R. Landry, and A. J. Miller (2013), Ecological transitions in a coastal upwelling ecosystem, *Oceanography*, *26*(3), 210–219.

Powell, J. R., and M. D. Ohman (2015), Co-variability of zooplankton gradients with glider-detected density fronts in the Southern California Current System, *Deep Sea Res., Part II*, *112*, 79–90, doi:10.1016/j.dsr2.2014.04.002.

Smith, C. R., D. J. Hoover, S. E. Doan, R. H. Pope, D. J. Demaster, F. C. Dobbs, and M. A. Altabet (1996), Phytodetritus at the abyssal seafloor across 10° of latitude in the central equatorial Pacific, *Deep Sea Res., Part II*, *43*(4-6), 1309–1338.

Strickland, J. D. H., and T. R. Parsons (1972), *A Practical Handbook of Seawater Analysis*, 2nd ed., 310 pp., Bull. of the Fish. Res. Board of Canada, Ottawa.

Stukel, M. R., M. D. Ohman, C. R. Benitez-Nelson, and M. R. Landry (2013), Contributions of mesozooplankton to vertical carbon export in a coastal upwelling system, *Mar. Ecol. Prog. Ser.*, *491*, 47–65.

Takeda, S. (1998), Influence of iron availability on nutrient consumption ratio of diatoms in oceanic waters, *Nature*, *393*(6687), 774–777.
Taylor, A. G., R. Goericke, M. R. Landry, K. E. Selph, D. A. Wick, and M. J. Roadman (2012), Sharp gradients in phytoplankton community structure across a frontal zone in the California Current Ecosystem, *J. Plankton Res.*, *34*(9), 778–789.
Thamatrakoln, K., and M. Hildebrand (2008), Silicon uptake in diatoms revisited: A model for saturable and nonsaturable uptake kinetics and the role of silicon transporters, *Plant Physiol.*, *146*(3), 1397–1407, doi:10.1104/pp.107.10704.
Yoder, J. A., S. G. Ackleson, R. T. Barber, P. Flament, and W. M. Balch (1994), A line in the sea, *Nature*, *371*(6499), 689–692.